Wire network behavior in superconducting Nb films with diluted triangular arrays of holes

2012 J. Phys.: Condens. Matter 24 155702

(http://iopscience.iop.org/0953-8984/24/15/155702)

J. Phys.: Condens. Matter **24** (2012) 155702 (7pp) doi:10.1088/0953-8984/24/15/155702

Wire network behavior in superconducting Nb films with diluted triangular arrays of holes

S K He, W J Zhang, H F Liu, G M Xue, B H Li, H Xiao, Z C Wen, X F Han, S P Zhao, C Z Gu and X G Qiu

Beijing National Laboratory for Condensed Matter Physics, Institute of Physics, Chinese Academy of Sciences, Beijing 100190, People's Republic of China

E-mail: xgqiu@aphy.iphy.ac.cn

Received 18 January 2012, in final form 25 February 2012
Published 22 March 2012
Online at stacks.iop.org/JPhysCM/24/155702

Abstract

We present results of transport measurements on superconducting Nb films with diluted triangular arrays (honeycomb and kagomé) of holes. The patterned films have large disk-shaped interstitial regions even when the edge-to-edge separations between nearest neighboring holes are comparable to the coherence length. Changes in the field interval of two consecutive minima in the field dependent resistance $R(H)$ curves are observed. In the low field region, fine structures in the $R(H)$ and $T_c(H)$ curves are identified in both arrays. Comparison of experimental data with calculation results reveals that these structures observed in honeycomb and kagomé hole arrays resemble those in wire networks with triangular and T_3 symmetries, respectively. The findings suggest that even in these specified periodic hole arrays with very large interstitial regions, the low field fine structures are determined by the connectivity of the nanostructures.

(Some figures may appear in colour only in the online journal)

1. Introduction

Superconducting films with periodic arrays of artificial pinning sites have been extensively studied for about two decades [1–4]. The so called commensurate effects such as peaks in the $I_c(H)$ curves and dips in the $R(H)$ curves can be observed at the fields where the number of superconducting flux quanta $\Phi_0 = hc/2e$ per unit area is an integer multiple of the number of pinning sites [3, 5, 6]. The most prevalent explanation for these effects is that the vortex lattice is commensurate with the underlying array and pinned efficiently at the matching fields.

However, similar phenomena have also been observed in other systems including superconducting wire networks and Josephson junction arrays [7–9]. In wire networks, when the magnetic flux through a single plaquette does not equal an integer multiple of Φ_0, supercurrents must be induced along the loops to satisfy the fluxoid quantization condition. There is an energy cost due to the induced supercurrents and this results in a reduced T_c. From this point of view, in wire networks, the resistance oscillations are caused by T_c suppression at non-matching fields rather than enhanced pinning at the matching fields [10]. Interestingly, transitions from the pinning regime to the wire network regime were observed in some pinning arrays [3, 11, 12].

We notice that these findings are based on square [3, 11, 12] and triangular [10] lattices. In those cases, with large dots (or holes) and small edge-to-edge separation, the remaining geometrical structures of the patterned films are indeed like wire networks which have narrow strands and small nodes. Thus the transition from pinning arrays to wire networks is straightforward. However, other series of hole arrays with large hole diameter may not have such direct geometrical simplification. Investigations of those hole arrays are needed to better understand and differentiate between the two mechanisms (vortex dynamics and phase coherence along the loops in wire networks) which lead to the commensurate effects.

In this work, superconducting Nb films with honeycomb and kagomé arrays of holes are studied. The arrays can be viewed as diluted triangular arrays, for they can be constructed with 1/3 and 1/4 of the sites removed form the original lattice, respectively [13]. The edge-to-edge separations between neighboring holes in these samples are comparable to the coherence length at temperature close to T_{c0}—although, unlike the case for square and triangular arrays, the patterned films still have large interstitial regions. This distinct character makes the arrays different from ideal wire networks in which a uniform order parameter in the cross section of any stripe is expected because the width of the stripes is smaller than the coherence length. Large interstitial regions, on the other hand, can facilitate the nucleation of Abrikosov vortices [2, 4, 14–18], resulting in the appearance of normal cores. In our experiments, a series of minima are observed in the $R(H)$ curves. While the oscillation period at low fields is in good agreement with the value derived from the hole density, the periodicity in higher fields is much larger. We found that the change of the spacing of minima is due to the presence of interstitial vortices in the high field region. Surprisingly, in the low field region, wire network behaviors are observed in both samples.

We identify the wire network behavior by the fractional matchings (fine structures) in the $R(H)$ and $T_c(H)$ curves. The positions and the relative values of the matching minima are studied in detail. We notice that the connectivity of a wire network determines the characters of the fine structures; therefore we highlight the connectivity of the hole arrays and simplify each of them to a wire network. The comparison of the results for the hole arrays with those for the corresponding wire networks, including reported experimental data as well as calculations based on the Alexander model [19], demonstrates that the hole arrays studied in this work are well described by wire networks when subjected to small field.

2. Experiment

The nanostructured superconducting films were prepared as follows. First, the superconducting Nb film with a thickness of 100 nm was deposited by magnetron sputtering on an Si substrate with an SiO_2 buffer layer. Next, a microbridge for four-terminal transport measurement was fabricated by ultraviolet photolithography followed by reactive ion etching. Then the desired arrays covering the whole bridge area of 60×60 μm^2 was patterned by electron-beam lithography on a polymethyl methacrylate (PMMA) resist layer. Finally, the pattern was transferred to the Nb film by magnetically enhanced reactive ion etching. In both the honeycomb and kagomé samples, the value of the center-to-center distance between nearest neighbors (a) is 400 nm and the hole diameter (d) is about 340 nm. The scanning electron micrograph image of the kagomé sample is shown in figure 1. The smallest width of the stripes between the adjacent holes is about 60 nm.

The transport measurements were carried out in a commercial physical properties measurement system (PPMS) manufactured by Quantum Design. The magnetic field was applied perpendicular to the film surface. During the measurements, the temperature stability was better than 2 mK. The zero-field transition temperatures $T_c(0)$ are 8.713 K for the honeycomb sample and 8.755 K for the kagomé sample, using a criterion of half the normal state resistance R_N at 9 K, namely 8.18 Ω and 9.02 Ω, respectively. The transition width of these two samples is about 0.15 K. The reference film without any pattern has a slightly higher T_c of 8.87 K and the transition width is only 50 mK. We have measured the $T_c(H)$ phase boundary of the reference sample and from the relation [20]

$$\mu_0 H_{c2} = \frac{\Phi_0}{2\pi\xi(0)^2}\left(1 - \frac{T}{T_c}\right), \qquad (1)$$

we obtained the zero-temperature coherence length $\xi(0) = 9.9$ nm.

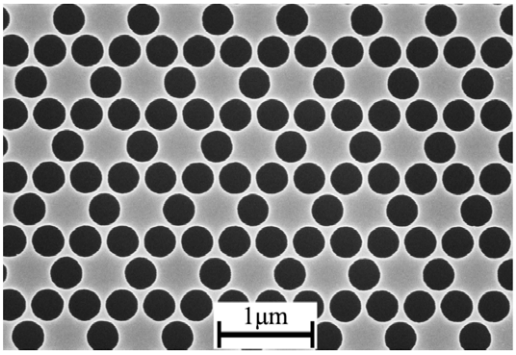

Figure 1. Scanning electron microscopy (SEM) image of the superconducting Nb film with a kagomé array of holes. The center-to-center distance between nearest neighbors is 400 nm and the hole diameter is about 340 nm.

3. Results and discussion

3.1. Reconfiguration

Figure 2 shows the $R(H)$ curve of the honeycomb sample measured at $T = 0.981T_c$ with a current of 50 μA. A series of local minima corresponding to primary matching as well as fractional ones are observed. Among these, seven primary matching minima can be clearly identified and their positions are indicated by the dashed lines. The field interval between two consecutive minima versus the corresponding index number is shown in the inset. At fields below 300 Oe, the observed intervals are about 96.5 Oe, in agreement with the value 99.6 Oe derived from the hole density. When the field is larger than the third matching field, the field spacing has a larger value of about 146.5 Oe. This value is very close to the matching field of a triangular lattice with the same lattice constant which is 149.4 Oe. One exception is that the spacing between the fourth and fifth minima is 100 Oe.

Figure 3 is the $R(H)$ curve of the kagomé sample measured at $T = 0.99T_c$ with a current of 10 μA. Several deep resistance minima can be identified and they are highlighted with dashed lines. As can be seen more clearly from the inset of figure 3, the field intervals have two sets of values too. The first three intervals are about 108.7 Oe, again in good

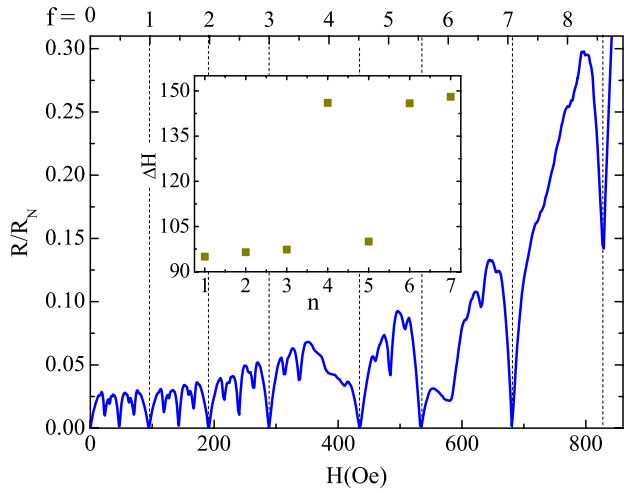

Figure 2. $R(H)$ curve of Nb film with a honeycomb array of holes measured at 8.55 K ($0.981T_c$) with a current of 50 μA. f is the filling ratio indicating the flux quanta per unit cell. The inset shows the field spacing of two consecutive minima as a function of the minima index.

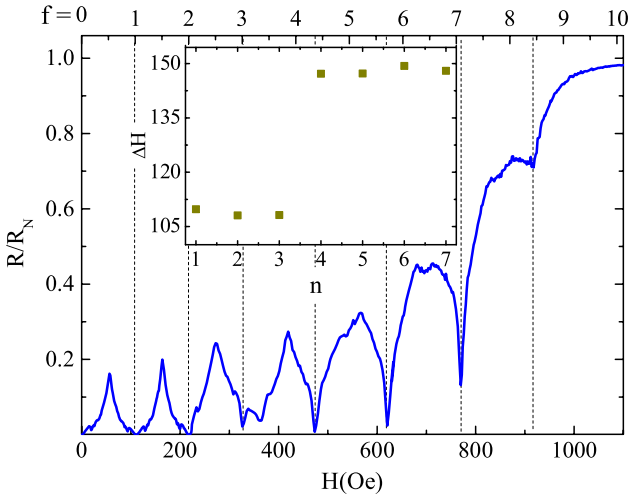

Figure 3. $R(H)$ curve of Nb film with a kagomé array of holes measured at 8.67 K ($0.99T_c$) with a current of 10 μA. f is the filling ratio indicating the flux quanta per unit cell. The inset shows the field spacing of two consecutive minima as a function of the minima index.

agreement with the first matching field ($H_1 = 112.1$ Oe) of the underlying kagomé lattice. However, the value of the intervals jumps to about 148 Oe when the field is larger than the third matching field.

The changes in the field intervals of two consecutive minima have been observed in rectangular arrays and have been explained in terms of reconfiguration of the vortex lattice from rectangular to square [2, 21]. The interstitial regions in rectangular arrays are stripes which lead to a channeling effect of the vortices [22, 23], while in honeycomb and kagomé arrays the interstitial regions have disk-like shape. At the typical measurement temperature 8.60 K, the diameters of the interstitial regions, approximately 520 nm, are about five times larger than the coherence length. Thus, Abrikosov vortices can be easily accommodated by the interstitial sites.

Form the field spacing values between two consecutive matchings, the overall feature of the $R(H)$ curves can be explained as follows. When the field is small, supercurrents are generated around the holes in order to satisfy the fluxoid quantization condition. At the integer matching field, it is the arrangement of the fluxoids that is commensurate with the hole lattice. When the applied magnetic field is larger than the third matching field, Abrikosov vortices are generated in the interstitial region to minimize the free energy [16]. These interstitial vortices are effectively pinned by the repulsive interactions from the fluxoids in the holes, which create a caging potential [24, 25]. The overall flux lattice, which is composed of interstitial vortices and the fluxoids in the holes, would have a triangular symmetry. That is why the field intervals of the minima observed in the high field region in both lattices are in good agreement with the value derived from a vortex lattice with a triangular arrangement. The saturation number n_s, namely, the maximum number of fluxoids trapped by one hole without the entry of interstitial vortices, is 3 for both samples. This value exceeds the limit $n_s = d/(4\xi(T)) \simeq 1$ given by Mkrtchyan and Schmidt [26], where d is the diameter of the defect and $\xi(T)$ is the temperature dependent coherence length. This fact indicates that the proximity of the holes is significant [27].

However, the exact vortex configurations and their evolution are strongly dependent on the density of flux quanta and the confinement of the mesoscopic structure. Both imaging experiments [4] and simulations [24, 28, 29] have revealed the complex nature of and the process of transition between various configurations of the composite vortex lattice. These features may also responsible for the observation of a field interval of 100 Oe between the fourth and fifth minima in figure 2.

3.2. Fractional matching and wire network behavior

In the low field region, fine and repeatable sub-minima are observed, as can be seen from figures 2 and 3. Because no interstitial vortex is involved in this region and because of the proximity of the holes, we can relate the systems to wire networks despite the large disk-shaped interstitial sites.

We notice that a wire network is obtained by assigning nodes to the center of the interstitial regions in the original hole array and connecting them. In figure 4, the centers of the interstitial regions are regarded as nodes. Then, the superconducting stripes between neighboring holes are viewed as wires (dotted lines) connecting the nodes. Following this procedure, the connectivity of the patterned films is highlighted and the honeycomb and kagomé hole arrays are transformed to triangular and T_3 wire networks, respectively. Although Abilio *et al* have found that superconducting Al film with a square array of holes can be described as a square wire network [30], the simplification that we made here is more radical, for the diameter of the disk-shaped interstitial regions is even larger than that of the holes. Assuming that the distance between the centers

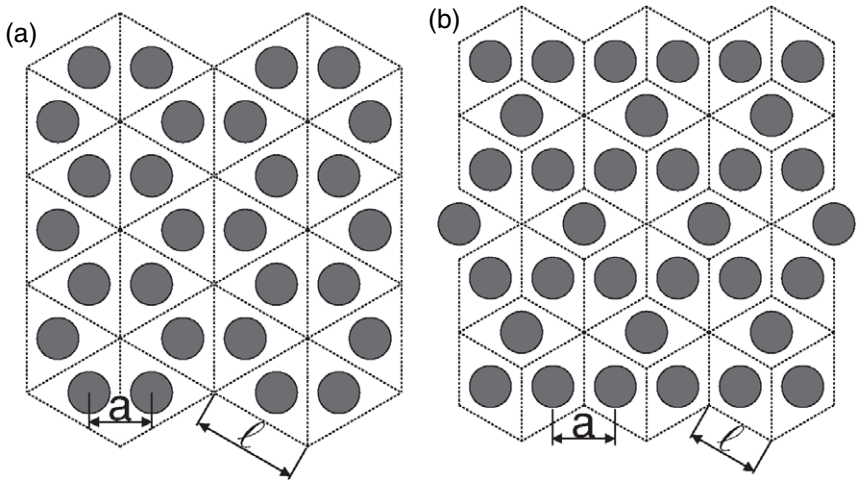

Figure 4. Illustration of the transformation from hole arrays (dark circles) to wire networks (dotted lines). (a) Honeycomb hole array to triangular wire network. (b) Kagomé hole array to T_3 wire network. a: the distance between the centers of the neighboring holes. l: the side length of the corresponding wire networks.

of the neighboring holes is a in the hole array, then in the dual lattices the side length l of the elementary triangles will be $\sqrt{3}a$ and the side length of the rhombus tile in the T_3 geometry will be $2\sqrt{3}a/3$, as can been seen from figure 4(a) and (b), respectively. If the matching effects of the hole arrays originate from T_c suppression at non-matching fields, the experimental results should show features similar to those that have been observed in their corresponding wire networks.

Figure 5(a) shows the fine structures of the $R(H)$ curve of the honeycomb sample measured at $T = 0.987T_c$ with a current of 10 μA. The x axis gives the filling ratio, $f = \Phi/\Phi_0$, where $\Phi = Ha^2 3\sqrt{3}/4$ is the magnetic flux per elementary triangle of the corresponding wire network. In the field range $0 \leq f \leq 1$, resistance minima are observed at $f = 1/4, 1/3, 1/2, 2/3$ and $3/4$. The magnitude of the oscillation is about eight per cent of R_N. At the field $f = 1/2$ where the commensurate effect is most pronounced, the resistance drops to a value comparable to that at zero field. At $f = 1/4$ and $3/4$, the resistances are about three per cent of R_N.

Figure 5(b) shows the $T_c(H)$ curves in reduced units, $\Delta T_c/T_c(0)$, versus f, using different resistance criteria $r = R/R_N$. The curves were obtained with a current of 10 μA. The parabolic background [7] which reflects the contribution of the finite width of the strands to the critical field has been subtracted. For $r = 0.05$ and 0.1, dips are observed at filling ratios $f = 1/4, 1/3, 1/2, 2/3$ and $3/4$. With the criterion of $r = 0.5$, only dips at $f = 1/4, 1/2$ and $3/4$ are visible and those at $f = 1/3$ and $2/3$ are missing. For $r = 0.8$, T_c changes smoothly with field and no features can be identified. Thus, comparing figures 5(a) and (b), one can see that minima in the $R(H)$ curve are located at the same fields where dips are observed in the $T_c(H)$ curve. The fine structures are more pronounced in $R(H)$ than in $\Delta T_c/T_c(0)$ versus f. This is because the resistance is measured at temperatures slightly above T_{c0} in the superconducting transition region where the resistance drops sharply with decreasing temperature; a small change in T_c will result in an enhanced effect in the resistance, and thus a more pronounced commensurate effect.

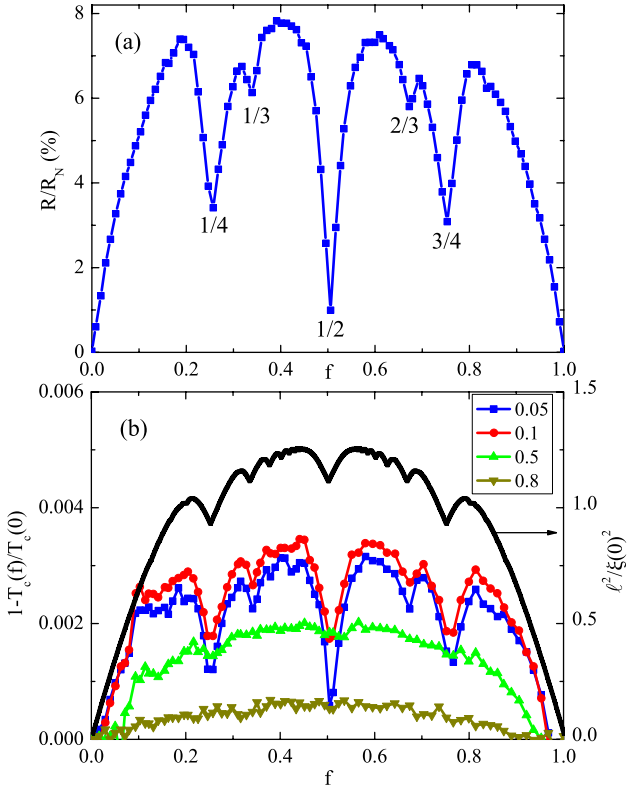

Figure 5. (a) Low field $R(H)$ curve for the sample with a honeycomb hole array measured at 8.60 K ($0.987T_c$) and $I = 10$ μA. The field is normalized by the first matching field and the resistance is normalized by R_N at 9 K. (b) The field dependent transition temperature $T_c(H)$ curves of the honeycomb sample with different criteria $r = R/R_N$. The parabolic background has been subtracted. The top one is the theoretical curve for a triangular wire network in units of $l^2/\xi(0)^2$.

To our knowledge, fractional matching effects in honeycomb arrays have only been observed at $f = 1/2$ in previous studies [13, 16]. At the typical measurement temperature $0.987T_c$ in this work, $\xi(T) = \xi(0)/\sqrt{1 - T/T_c} = 86.9$ nm

is slightly larger than the width of the narrow stripes. This fact makes the samples investigated here qualitatively different from those in previous works on hole arrays and better described as wire networks. Rich structures in the $T_c(H)$ curves of wire networks may serve as fingerprints for differentiating one array from another, since for a given geometry the fine structures are only expected at a particular series of filling ratios [7, 31, 32]. From the linearized Ginzburg–Landau equations, Alexander had derived the relation of the order parameters at the nodes subjected to non-integer flux [19]. On the basis of those equations, the task of finding the field dependent transition temperature is reduced to eigenvalue problems. The mathematical treatment is very similar to that of the tight binding electrons in 2D arrays subjected to an external field, which leads to the famous Hofstadter butterfly energy spectrum [33]. The top curve plotted in figure 5(b) shows the theoretical values of $T_c(H)$ for the triangular wire network, which is the structure dual to the honeycomb hole array. The curve is calculated by using

$$\frac{T_c(0) - T_c(f)}{T_c(0)} = \frac{\xi(0)^2}{l^2}\left(\arccos\frac{\varepsilon_t}{6}\right)^2, \qquad (2)$$

where l is the side length of the wires, ε_t is the eigenvalue [19] of the following equation obtained by using the Landau gauge and periodic boundary conditions:

$$\begin{aligned}\varepsilon_t\psi_n = {} & 2\cos[\pi(2n-1)f - k_y/2]e^{-ik_y/2}\psi_{n-1} \\ & + 2\cos[4\pi nf - k_y]\psi_n + 2\cos[\pi(2n+1)f - k_y/2] \\ & \times e^{ik_y/2}\psi_{n+1}, \end{aligned} \qquad (3)$$

where $k_y = 2\pi\frac{k-1}{N}, k = 1, \ldots, N$, implies the periodic condition, n denotes the node index and ψ_n is the order parameter at node n. The fine structures of $T_c(H)$ for the triangular wire network have also been studied by an analytical approach based on multiple-loop Aharonov–Bohm Feynman path integrals [31]. The main features in $T_c(H)$ such as the position and relative strength of the most prominent dips are the same as those in Alexander's treatment. The most pronounced dips occur at $f = 1/4, 1/3, 1/2$ etc, in good agreement with the experimental data. At the fields where dips are observed, the order parameters at the nodes interfere constructively and form different locked-in states corresponding to local maxima in T_c [34]. In the fabrication process, contamination and damage of the samples are most significant for the narrow strips, resulting in a lower T_c and a widening in the transition width compared to that of the reference film. The phase coherence between adjacent nodes is fully established when all the stripes are in a superconducting state. Therefore, the interference effect is strong near the zero-resistance state $r = 0.05$ and significantly reduced for $r > 0.1$.

Figure 6(a) shows the low field $R(H)$ curve of the kagomé sample measured at $T = 0.99T_c$. With the kagomé geometry, f corresponds to the magnetic flux through a rhombic tile with side length $2\sqrt{3}a/3$: $f = \Phi/\Phi_0 = 2\sqrt{3}a^2H/(3\Phi_0)$. Again we focus on the results for f in the interval between 0 and 1. Dips are identified at $f = 1/6, 2/9, 7/9$ and $5/6$. These fine structures are observed for the first time in a kagomé

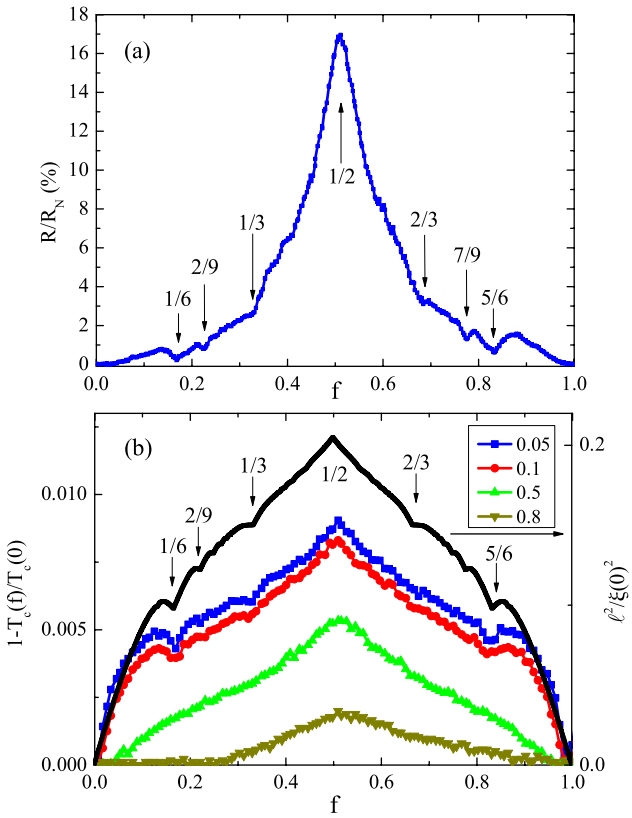

Figure 6. (a) Low field $R(H)$ curve for the sample with a kagomé array measured at 8.67 K ($0.99T_c$) and $I = 10$ μA. (b) The field dependent transition temperature $T_c(H)$ of the kagomé sample with different criteria $r = R/R_N$. The parabolic background has been subtracted. The top one is the theoretical curve for the T_3 wire network in units of $l^2/\xi(0)^2$ [35].

hole array, perhaps because of the specified geometrical parameters. Anomalies are also visible at $f = 1/3$ and $2/3$, but they are more like kinks than dips. Most strikingly, in contrast to the dip observed in the honeycomb sample, a remarkable peak is observed at $f = 1/2$. The resistance is far above the background, reaching 16.9% of the normal state resistance.

Figure 6(b) shows the $T_c(H)$ curves in reduced units, $\Delta T_c/T_c(0)$, versus f, for the kagomé sample determined by using different criteria for r. Again, all the measurements were carried out with a current of 10 μA. For small values of r (0.05 and 0.1), dips are present at $1/6$, $2/9$, $1/3$, $2/3$ and $5/6$, although the one at $2/3$ is relatively weak (see the labels in figure 6(b)). For larger values of r (0.5 and 0.8), the dips at $1/6$, $2/9$ and $1/3$ gradually disappear, but the peak at $f = 1/2$ remains pronounced.

Most of the fractional matchings observed here are absent in previous works performed on kagomé lattice [13, 25, 36–38]. In a recent work on hole arrays with small hole size which is in the pinning regime limit, clear fractional matchings were only observed at $f = 1/3$ and $2/3$ [38]. Contrasting with their findings, in our work with edge-to-edge separation comparable to the coherence length, the dips at $f = 1/6$ and $5/6$ are most pronounced and a distinct peak anomaly at $f = 1/2$ is observed. The results agree well with what has been observed in T_3 wire networks [35, 39], the

structure dual to the kagomé hole array as seen in figure 4(b). The top curve of figure 6(b) shows the theoretical curve for T_3 networks [35]. This is obtained from the following equation which relates the eigenvalues of T_3 ($\varepsilon(f)$) at filling ratio f to the eigenvalues for the triangular lattice at $3f/2$ [35]:

$$\varepsilon^2(f) - 6 = 2\cos(\pi f)\varepsilon_t(3f/2). \quad (4)$$

The comparison with the theoretical curve shows that only the dips at $f = 7/9$ and other weaker ones are absent in the experimental curves. For $f = 1/6, 2/9$ and $1/3$, constructive interference occurs among the superconducting order parameters of the interstitial sites and the fluxoids establish long range locked-in commensurate order, while for $f = 1/2$, superconductivity is localized in single tiles and long range coherence between network sites cannot be established [35]. This kind of fully destructive quantum interference has also been observed in kagomé wire networks [34, 40]. The oscillation of the $R(H)$ curve with a peak at half a flux per tile is similar to the single-loop Little–Parks effect. In that case, the supercurrent density must reach the largest value at half a flux in order to satisfy the fluxoid quantization condition [41].

The results obtained from these two lattices confirm the validity of the transform from a hole array to a wire network. However, in contrast to the ideal wire networks or square arrays of holes having small nodes, the geometries studied here possess very large superconducting disk-shaped nodes which can trap Abrikosov vortices easily. The formation of Abrikosov vortices implies spatial variation and the presence of zero points of the order parameters in the interstitial region. Then the simplification of the large interstitial region to a node in a wire network is no longer appropriate. Therefore, transformation from hole arrays to wire networks is only valid for small field values.

4. Conclusions

In conclusion, we have studied the commensurate effects in superconducting films with honeycomb and kagomé arrays of holes with small edge-to-edge separation. We found that the magnetoresistance curves have two regions with different oscillation periods. At small fields, there are no Abrikosov vortices present in the interstitial regions. The large disk-shaped interstitial region can be simplified as a single node and a one-to-one correspondence between hole arrays and wire networks is established. Comparison of experimental data with calculation shows that the simplification works well. Our results suggest that at low fields, the behaviors of these specified periodic hole arrays are determined by the connectivity of the systems.

Acknowledgments

We thank Q Niu, X C Xie, B Y Zhu and Y Yeshurun for fruitful discussion. This work was supported by National Basic Research Program of China (Nos 2009CB929100, 2011CBA00107, 2012CB921302) and the National Science Foundation of China (Nos 91121004, 10974241, 11104335).

References

[1] Baert M, Metlushko V V, Jonckheere R, Moshchalkov V V and Bruynseraede Y 1995 *Phys. Rev. Lett.* **74** 3269
[2] Martin J I, Velez M, Hoffmann A, Schuller I K and Vicent J L 1999 *Phys. Rev. Lett.* **83** 1022
[3] Hoffmann A, Prieto P and Schuller I K 2000 *Phys. Rev.* B **61** 6958
[4] Karapetrov G, Fedor J, Iavarone M, Rosenmann D and Kwok W K 2005 *Phys. Rev. Lett.* **95** 167002
[5] Van Look L, Zhu B Y, Jonckheere R, Zhao B R, Zhao Z X and Moshchalkov V V 2002 *Phys. Rev.* B **66** 214511
[6] Martin J I, Velez M, Nogues J and Schuller I K 1997 *Phys. Rev. Lett.* **79** 1929
[7] Pannetier B, Chaussy J, Rammal R and Villegier J C 1984 *Phys. Rev. Lett.* **53** 1845
[8] Ling X S *et al* 1996 *Phys. Rev. Lett.* **76** 2989
[9] Tinkham M, Abraham D W and Lobb C J 1983 *Phys. Rev.* B **28** 6578
[10] Patel U, Xiao Z L, Hua J, Xu T, Rosenmann D, Novosad V, Pearson J, Welp U, Kwok W K and Crabtree G W 2007 *Phys. Rev.* B **76** 020508
[11] Bruynseraede Y, Puig T, Rosseel E, Baert M, Van Bael M, Temst K, Moshchalkov V V and Jonckheere R 1997 *J. Low Temp. Phys.* **106** 173
[12] Moshchalkov V V, Baert M, Metlushko V V, Rosseel E, Van Bael M J, Temst K, Bruynseraede Y and Jonckheere R 1998 *Phys. Rev.* B **57** 3615
[13] Reichhardt C and Reichhardt C J O 2007 *Phys. Rev.* B **76** 064523
[14] Harada K, Kamimura O, Kasai H, Matsuda T, Tonomura A and Moshchalkov V V 1996 *Science* **274** 1167
[15] Metlushko V *et al* 1999 *Phys. Rev.* B **60** R12585
[16] Wu T C, Wang J C, Horng L, Wu J C and Yang T J 2005 *J. Appl. Phys.* **97** 10B102
[17] Kramer R B G, Silhanek A V, Van de Vondel J, Raes B and Moshchalkov V V 2009 *Phys. Rev. Lett.* **103** 067007
[18] Grigorenko A N, Bending S J, Van Bael M J, Lange M, Moshchalkov V V, Fangohr H and de Groot P A J 2003 *Phys. Rev. Lett.* **90** 237001
[19] Alexander S 1983 *Phys. Rev.* B **27** 1541
[20] Tinkham M 1996 *Introduction to Superconductivity* 2nd edn (Singapore: McGraw-Hill) p 135
[21] Martin J I, Velez M, Hoffmann A, Schuller I K and Vicent J L 2000 *Phys. Rev.* B **62** 9110
[22] Velez M, Jaque D, Martin J I, Montero M I, Schuller I K and Vicent J L 2002 *Phys. Rev.* B **65** 104511
[23] Villegas J E, Gonzalez E M, Montero M I, Schuller I K and Vicent J L 2003 *Phys. Rev.* B **68** 224504
[24] Berdiyorov G R, Milosevic M V and Peeters F M 2006 *Phys. Rev. Lett.* **96** 207001
[25] Reichhardt C and Reichhardt C J O 2009 *Phys. Rev.* B **79** 134501
[26] Mkrtchyan G S and Schmidt V V 1972 *Sov. Phys.—JETP* **34** 195
[27] Doria M M, de Andrade S C B and Sardella E 2000 *Physica* C **341–348** 1199
[28] Reichhardt C J O, Libál A and Reichhardt C 2006 *Phys. Rev.* B **73** 184519
[29] Berdiyorov G R, Milošević M V and Peeters F M 2006 *Phys. Rev.* B **74** 174512
[30] Abilio C C, Amico L, Fazio R and Pannetier B 2000 *J. Low Temp. Phys.* **118** 23
[31] Lin Y-L and Nori F 2002 *Phys. Rev.* B **65** 214504
[32] Erdős P and Zheng W 2010 *Phys. Rev.* B **82** 134532

[33] Hofstadter D R 1976 *Phys. Rev.* B **14** 2239
[34] Higgins M J, Xiao Y, Bhattacharya S, Chaikin P M, Sethuraman S, Bojko R and Spencer D 2000 *Phys. Rev.* B **61** R894
[35] Abilio C C, Butaud P, Fournier T, Pannetier B, Vidal J, Tedesco S and Dalzotto B 1999 *Phys. Rev. Lett.* **83** 5102
[36] Morgan D J and Ketterson J B 1998 *Phys. Rev. Lett.* **80** 3614
[37] Laguna M F, Balseiro C A, Domínguez D and Nori F 2001 *Phys. Rev.* B **64** 104505
[38] Cuppens J, Ataklti G W, Gillijns W, Van de Vondel J, Moshchalkov V V and Silhanek A V 2011 *J. Supercond. Nov. Magn.* **24** 7
[39] Vidal J, Mosseri R and Douçot B 1998 *Phys. Rev. Lett.* **81** 5888
[40] Xiao Y, Huse D A, Chaikin P M, Higgins M J, Bhattacharya S and Spencer D 2002 *Phys. Rev.* B **65** 214503
[41] Little W A and Parks R D 1962 *Phys. Rev. Lett.* **9** 9